High-Accuracy Localization for Assisted Living

Klaus Witrisal, Paul Meissner, Erik Leitinger, Yuan Shen,
Carl Gustafson, Fredrik Tufvesson, Katsuyuki Haneda,
Davide Dardari, Andreas Molisch, Andrea Conti, and Moe Z. Win

***Abstract*—Assisted living (AL) technologies, enabled by technical advances such as the advent of the Internet-of-Things, are increasingly gaining importance in our ageing society. This article discusses the potential of future high-accuracy localization systems as a key component of AL applications. Accurate location information can be tremendously useful to realize, e.g., behavioral monitoring, fall detection, and real-time assistance. Such services are expected to provide older adults and people with disabilities with more independence and thus to reduce the cost for caretaking.**

Total cost of ownership and ease of installation are paramount to make sensor systems for AL viable. In case of a radio-based indoor localization system, this implies that a conventional solution is unlikely to gain widespread adoption because of its requirement to install multiple fixed nodes (anchors) in each room. This paper therefore places its focus on (i) discussing radiolocalization methods that reduce the required infrastructure by exploiting information from reflected multipath components and (ii) showing that knowledge about the propagation environment enables localization with high accuracy and robustness. It is demonstrated that new millimeter-wave (mm-wave) technology, under investigation for 5G communications systems, will be able to provide cm-accuracy indoor localization in a robust manner, ideally suited for AL.

***Index Terms*—Assisted living technologies, location awareness, location aware communications, ultra wideband systems, mm-wave systems, localization, tracking, positioning, Cramér-Rao bounds, channel models**

I. Introduction

The robust provisioning of accurate location information is a key enabler for AL systems. A recent survey on ambient intelligence in healthcare [1] illustrates the wide range of applications that could be supported by a cm-accuracy indoor positioning system *alone*: Activity recognition, behavioral pattern discovery, anomaly detection, and decision support methods can all be based on such a sensor modality. Application examples include behavioral monitoring to assess the physical and mental health of individuals, emergency (fall) detection to alert caretakers or emergency services, real-time assistance to provide context awareness to medication management systems (to remind—for instance—to take medications before/during/after meals) or as an orthotic and rehabilitation tool for individuals suffering from cognitive decline, geofencing for people with dementia, and even as a navigation aid for visually impaired (see [1] and the references therein).

However, as of today, the technologies for indoor localization have not converged towards a unique winning approach, hence the topic is still subject of research and competitions [2]. Among the many location sensing methods proposed [3]–[9], active or passive radiolocalization[1] are most promising, because radio transceivers can be integrated in existing devices like smartphones and built at small form factors with low power consumption. Video cameras and microphones [11]–[13], for example, suffer from occlusions and a lack of acceptance because of privacy concerns. But the influence of the dense multipath radio channel in indoor environments still makes accurate and robust radiolocalization a challenging task. Ultra-wideband (UWB) signals have been shown to deliver excellent accuracy, since they allow for a separation of the multipath components (MPCs) [14]–[17]. Hence, on the one hand, the direct signal path can be isolated from interfering MPCs; on the other hand, position-related information in later-arriving MPCs becomes accessible as well and turned into an advantage [18].

Unfortunately, dedicated technology is required to implement traditional UWB systems operating in the microwave band (at $3.1 - 10.6$ GHz). With the advent of mm-wave communications in the 60 GHz band [19]–[21], a UWB localization system could operate synergetically with an existing communication system, e.g. using the IEEE 802.11ad standard [22]. Furthermore, 60 GHz regulations allow much higher transmit power compared to microwave UWB systems. Beamforming technologies proposed for these systems [19] perfectly complement the needs of the localization system and vice versa: also the beamforming algorithms will benefit from the location information and from environmental radio maps, i.e. spatial characterizations of the propagation channel that can be estimated and tracked in realtime. Location awareness is created, which is beneficial for different layers of the protocol stack of a communications system [23].

The reduction of the required infrastructure is of key importance for a viable localization system for AL. At the same time, localization with high accuracy and robustness is needed. This paper discusses a range of multipath-assisted localization approaches that actively take environmental propagation information into account to cope with these seemingly conflicting requirements. Even with only *a single anchor node* within each room, highly-accurate and robust location estimates can be obtained [18], [24], [25]. As a side effect, this method also reduces the amount of electromagnetic radiation, possibly increasing its acceptance by users. High accuracy and robustness are more easily achieved with active systems [18], [24] where the user has to wear e.g. a bracelet as illustrated in Fig. 1, while passive systems [25], [26] prevent the risk of lacking user compliance.

[1]In active localization, devices to be localized are equipped with a radio device participating in the communication, which is not the case in passive localization [10].

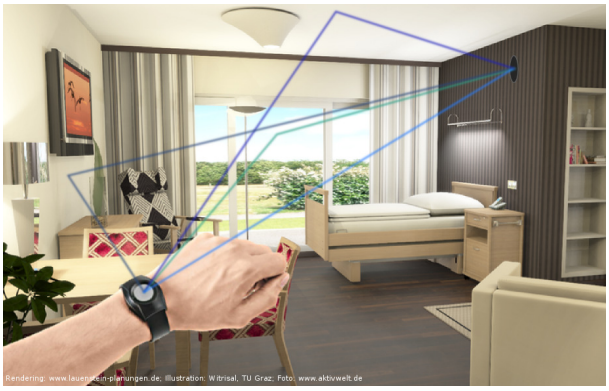

Fig. 1. Illustration of a high-accuracy, multipath-enabled indoor localization system for assisted-living applications. Information from reflected signals (such as the exemplary rays depicted) can be exploited if the geometry of the environment is taken into account.

This paper highlights the following issues:

- A model of the received signal using a geometry-based stochastic channel model and the concept of virtual sources/anchors. This leads to an *environment model* that describes the localization capability in a specific environment.
- Performance limits for indoor localization employing multipath propagation, showing the relevance of geometrically modeled MPCs.
- Algorithms for multipath-assisted localization and tracking: Maximum likelihood localization, tracking filters with data association, algorithms for passive localization and multi-target identification.
- Experimental and numerical results demonstrating the localization accuracy and robustness using a current experimental microwave-band system and the potential performance of a mm-wave system.
- Discussions and conclusions, evaluating the usefulness of the presented concepts for accurate and robust localization as a key component of an AL system.

Creating the proposed infrastructure, developing the appropriate distributed processing algorithms, and validating the applications in challenging AL environments will require significant multidisciplinary work over the coming years.

The remainder of this paper is structured as follows: Section II discusses the signal modeling and the resulting performance bounds for multipath-assisted localization. The separated text box (now in the appendix) contains details on the models and derivations. An extensive overview over multipath-assisted localization and tracking algorithms together with representative results is found in Section III, while the discussion of mm-wave systems for localization is given in Section IV. The paper is wrapped up with a summary and conclusions in Section V.

II. Signal Models and Performance Bounds

A suitable signal model supporting the analysis of a multipath-assisted localization system requires a description of the geometry to address the position dependence of signal features and stochastic elements to represent signal impairments and noise. We hence use a geometry-based stochastic channel model to describe the signal transmitted from a mobile agent node to a fixed anchor node (or the other way around, from anchor to agent). The received signal is thus modeled as a convolution of a UWB transmit pulse $s(t)$ with the channel

$$r(t) = \sum_{k=1}^{K} \alpha_k s(t-\tau_k) + s(t) * \nu(t) + w(t), \qquad (1)$$

where the sum accounts for K deterministic MPCs with complex amplitudes $\{\alpha_k\}$ whose delays $\{\tau_k\}$ yield useful position-related information, while the stochastic process $\nu(t)$ represents diffuse multipath (DM) which is *interference* to these useful components. The signal $w(t)$ denotes white Gaussian measurement noise at power spectral density (PSD) N_0. We assume a unit-energy pulse $s(t)$, such that the energy of the k-th MPC is given as $|\alpha_k|^2$. DM is everything that is not or can not be described by the deterministic components. It is modeled as a (Gaussian) random process with auto-covariance $\mathrm{E}\{v(t)v^*(\tau)\} = S_\nu(\tau)\delta(t-\tau)$, where $S_\nu(\tau)$ is a power delay profile (PDP) accounting for the non-stationary variance of the DM in the delay domain [27].

We assume that the result of a possible linear beamformer is already incorporated in $r(t)$. Beamforming will have an impact on the energies $|\alpha_k|^2$ and the DM, but for simplicity we do not indicate these dependencies in our equations.

To describe the *localization environment*, we propose a model for the signal-to-interference-plus-noise ratios (SINRs) of MPCs along with their propagation delays. The delays are deterministically related to the geometry at hand. We model the delay τ_k of the k-th MPC using a virtual anchor (VA) [18], [28] at position $\mathbf{a}_k$, yielding $\tau_k = \frac{1}{c}\|\mathbf{p} - \mathbf{a}_k\|$, where $\mathbf{p}$ is the position to be determined and c is the speed of light. For reflections at plane surfaces, the positions of the VAs can be computed straightforwardly: physical anchors are simply mirrored w.r.t. the planes; iterated mirroring operations account for higher-order reflections [27].

The SINR of the k-th component is defined as

$$\mathrm{SINR}_k = \frac{|\alpha_k|^2}{N_0 + T_\mathrm{p} S_\nu(\tau_k)}, \qquad (2)$$

relating the *useful* MPC energy $|\alpha_k|^2$ to the combined effects of the noise and the *interfering* DM. The latter is characterized by its PDP at the corresponding delay. The influence of the DM scales with the effective pulse duration T_p, i.e. with the inverse of the bandwidth of the measurement signal.

The model for the received signal in (1) enables the derivation of a Cramér-Rao lower bound (CRLB) on the position estimation error. (The derivation is briefly discussed in a boxed text block; see the appendix of this manuscript.) Using the information inequality, we obtain the position error bound (PEB) $\mathbb{E}_{\mathbf{r}|\mathbf{p}}\left\{\|\hat{\mathbf{p}} - \mathbf{p}\|^2\right\} \geq \mathrm{tr}\{\mathbf{J}_\mathbf{p}^{-1}\}$, where $\hat{\mathbf{p}}$ is the estimated position and $\mathbf{J}_\mathbf{p}$ is the equivalent Fisher information matrix (EFIM) of the position vector [29]–[31]. The EFIM can be written—under the assumption of resolvable, "non-overlapping" MPCs (see also the boxed text (appendix))—in the form [27], [32]

$$\mathbf{J}_\mathbf{p} = \frac{8\pi^2\beta^2}{c^2} \sum_{k=1}^{K} \mathrm{SINR}_k \mathbf{J}_r(\phi_k), \qquad (3)$$

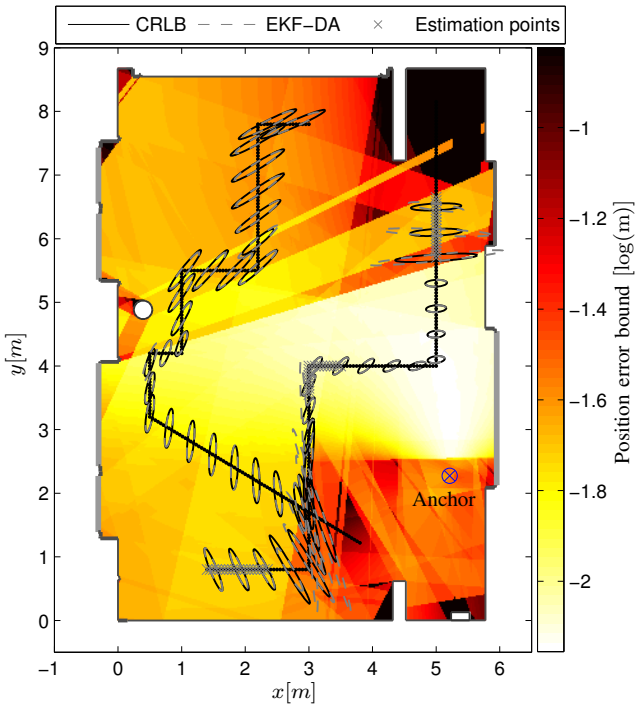

Fig. 2. Position error bound (PEB) and tracking results for $T_\mathrm{p} = 0.5\,\mathrm{ns}$, $f_\mathrm{c} = 7\,\mathrm{GHz}$, and a single fixed anchor. The PEB (3) has been computed from estimated SINRs (2); grey crosses are 60 positions used for this SINR estimation [18]. Solid and dashed ellipses denote the standard deviation ellipses corresponding to the CRLB and to the error covariance matrices of an extended Kalman tracking filter, respectively, at several points along two trajectories. These ellipses are enlarged by a factor of 20 for better visibility.

where β denotes the effective (RMS) bandwidth of the measurement signal and $\mathbf{J}_r(\phi_k)$ is a rank-one matrix with an eigenvector pointing along the angle of arrival (AoA) ϕ_k of the k-th MPC. This simple, canonical form of the EFIM allows for important conclusions regarding localization:

- Each geometrically modeled (deterministic) MPC yields additional position-related information which is quantified by its SINR value. In fact, the range $\hat{d}_k$ estimated from the k-th MPC has an error variance bounded as $\mathrm{var}\left\{\hat{d}_k\right\} \geq c^2/(8\pi^2\beta^2\mathrm{SINR}_k)$; i.e. the SINRs indicate the uncertainties of the MPC ranges.
- The equations relate to the system parameters (e.g. bandwidth expressed by β and T_p), the environment model (the SINR values), and the geometry (the AoAs) and thus indicate the expected performance *in a specific scenario*.

Figure 2 shows an evaluation of the PEB according to (3) for a single fixed anchor, for SINR values estimated from measured channel impulse response data [33]. The evaluation takes into account the visibility of the VAs across the floor plan but it assumes a "global" model of SINRs for the entire room shown[2]. Two-dimensional positioning is considered here; the measurement data have been acquired over a bandwidth of 2 GHz at a 7 GHz carrier [33]. According to this result, the expected precision lies in between one and ten centimeters for most of the area.

The figure provides a prediction of the spatial distribution of the achievable performance. It can thus be considered as an indication for the robustness of the localization system for a specific environment. As mentioned in Section II, the set of VAs and the quantification of their relevance as given by the SINR model represents an *environment model* which reflects the potential localization accuracy. Using (2) and (3), the influence of system parameters, such as the signal bandwidth, can be quantified.

III. Algorithms for Multipath-Assisted, Environment-Aware Localization

For the practical application of a multipath-assisted positioning and tracking system, two core challenges need to be tackled. (i) Algorithms are needed that can properly exploit the position-related information provided by each MPC; and (ii) algorithms are needed that can estimate the required side information, i.e. the environment model. Efficient solutions must be able to capture the relevant information from measurements at a reasonable computational complexity.

A. Multipath-assisted Localization and Tracking

Fig. 3 shows the block diagram of a multipath-assisted tracking scheme that is based on a Bayesian tracking filter [18], [33]. A core component of this scheme is the data association block. It associates, at each timestep n, the arrival times of a number of MPCs to the predicted delays. The arrival times (collected in the set $\mathcal{Z}_n$) are estimated from the received signal $r_n(t)$ by a high-resolution maximum-likelihood channel estimation algorithm; the predicted delays are computed from the VA positions $\{\mathbf{a}_k\}$ (collected in the set $\mathcal{A}_n$) and the predicted agent position $\hat{\mathbf{p}}_n^-$. The data association is needed to identify the potential (virtual) signal sources, to discard false detections due to dense multipath, and to ignore missing arrival-time measurements. It has been accomplished in [18], [33] using a constrained optimal subpattern assignment approach [35]. This means that the predicted and estimated MPC delays are matched using combinatorial optimization with the constraint that associations at a distance larger than a so-called cut-off distance are discarded. The output of the data association block, i.e the positions of the associated VAs $\mathcal{A}_{n,\mathrm{ass}}$ and corresponding MPC delays $\mathcal{Z}_{n,\mathrm{ass}}$, are fed into the tracking algorithm as measurement inputs.

In the upper branch of the block diagram, the SINR model is updated, which reflects the *reliability* of the range measurements: the SINRs are estimated using past measurements of the MPC amplitudes [34]. The SINRs can also be estimated from offline training data [18]. Using this side information, the tracking filter can perform an appropriate measurement weighting of the extracted delays [18]. Furthermore, the SINRs allow for relevance determination: the overall set of VAs $\mathcal{A}_n$ can be reduced to a set of relevant VAs $\tilde{\mathcal{A}}_n$. Also geometric considerations, like the visibilities of certain VAs, can be incorporated at this stage [33].

Fig. 4 illustrates the efficiency of this approach based on experimental data in the microwave-UWB band at a bandwidth

[2]To create a more detailed picture, one could estimate individual SINR-sets for different parts of a room or even estimate the SINR values online [34].

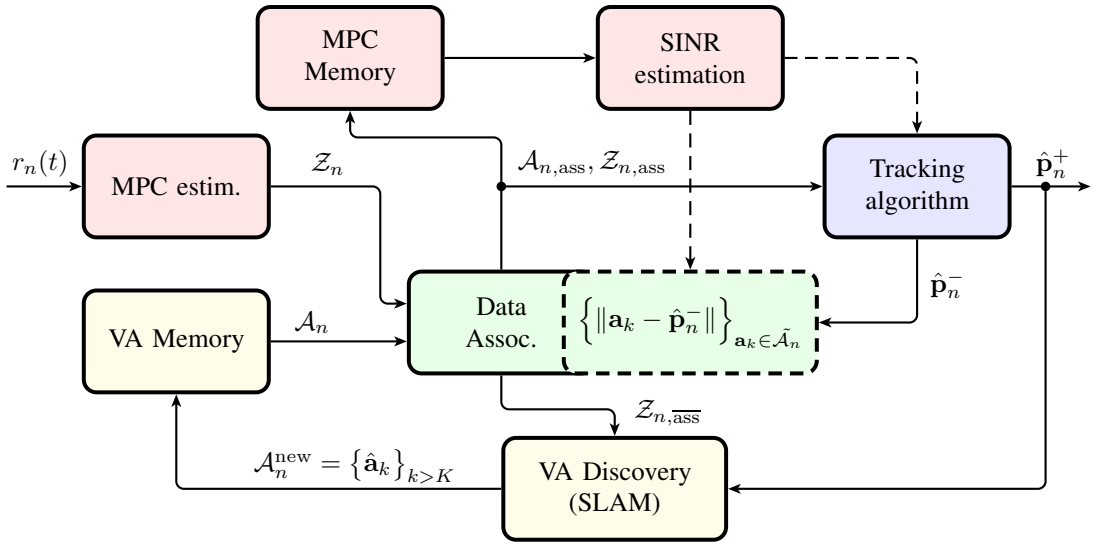

Fig. 3. Block diagram of state space tracking and data association scheme using MPC range estimates. The input is the received signal $r_n(t)$, the overall output the estimated agent position $\hat{\mathbf{p}}_n^+$ at timestep n. The estimation is performed using the environment model represented by the memory blocks.

of 2 GHz [18], [33]. It compares the CDFs of the position errors for algorithms having different levels of environment models available. The data have been obtained on 25 measurement trajectories with two fixed anchors. Trajectory points were spaced by 5 cm, while the different trajectories were obtained by shifting the entire tracks in 1 cm steps. An algorithm that exploits SINR information (red curves) obtains excellent robustness *and* accuracy: all 25 runs have similar performance with 90 % of the errors below 4 cm. Without SINR information (black and gray), 10 of 25 runs diverge. This occurs mostly in a short part of the trajectory where the LOS to one of the anchors is lost, being a strong indication of a reduced robustness. The overall CDF for the 15 non-diverging runs is shown by the black bold dashed line; 90 % of the errors are within 7 cm. Tracking results are also observable in Fig. 2, showing two example trajectories and the performance using only a single anchor. The standard deviation ellipses of the tracking filter match those corresponding to the CRLB and indicate the relevance of position information available in different directions.

Fig. 4 also shows the influence of a correction of the VA positions which has been done to refine the environment model in comparison to a VA model computed from the floorplan. A maximum a-posteriori (MAP) estimator has been used for this refinement, employing a set of training data at known locations. The performance without this MAP refinement is indicated by the blue dash-dotted curve. It shows a similar robustness but a reduced accuracy. We see this result as an evidence that the SINR model improves the robustness, while the VA-position refinement is needed to optimize the accuracy.

The environment model, e.g. the SINR information, thus is the key to obtain *efficient* tracking algorithms; not only in terms of achieving optimal performance, but also in terms of complexity: The set of relevant VAs in a scenario is significantly smaller than the overall set of VAs that would be taken into account by visibility considerations [18][3]. By

[3]Usually, the number of MPCs carrying relevant information is on the order of 5–10 per radio link.

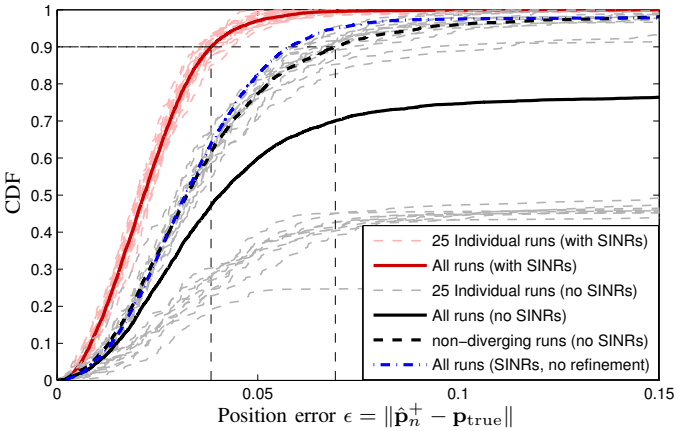

Fig. 4. Performance CDFs for $T_{\mathrm{p}} = 0.5\,\mathrm{ns}$ and $f_{\mathrm{c}} = 7\,\mathrm{GHz}$. Thin dashed lines show the individual 25 runs over the trajectories. Red and gray indicate the performance of the EKFs with and without estimated SINRs. Bold lines denote the total performance for all runs, the dashed line indicates the performance without SINRs on all non-diverging runs (15 out of 25).

also considering the uncertainty of the VA positions in the environment model, i.e. including the VAs to the state space, the position refinement can be done online at low complexity [34], eliminating the need for training measurements. Processing steps such as environment model tracking and relevance determination are potential features of a *cognitive* localization system. "Cognition" is aimed at understanding the surrounding world as found for instance in human visual perception (cf. [36], [37]).

The presented tracking approach naturally makes use of the position estimate obtained in the previous time step. Hence, an initialization strategy is also needed, i.e. a *localization* algorithm. Reference [24] proposes a maximum likelihood estimation algorithm based on (4). The important role of DM is taken into account by directly estimating the corresponding PDP $S_\nu(\tau)$ from the sampled received signals. No data association is necessary, since the entire received signal is used. In this way, a similar performance is achieved as in Fig. 4.

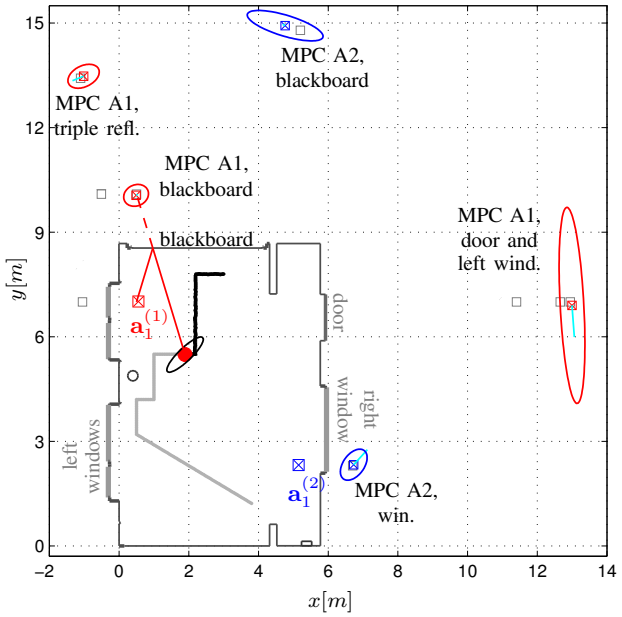

Fig. 5. Illustration of the environment map obtained by a SLAM algorithm. Two anchors at $\mathbf{a}_1^{(1)}$ and $\mathbf{a}_1^{(2)}$ represent the infrastructure. The agent position as well as the floor plan (represented by virtual anchors (VAs)) are estimated using specular multipath, for which one example path is shown. Grey squares indicate geometrically expected VAs, blue and red square-cross markers with uncertainty ellipses (30-fold) represent discovered VAs. An agent tracking result is shown in black with an error ellipse (100-fold).

Examples of the likelihood as a function of position $\mathbf{p}$ are shown in Section IV for mm-wave measurements.

This maximum likelihood approach can also be used in a tracking manner, resulting in particle-filter-based implementations of the scheme in Fig. 3. Although such algorithms have increased computational complexity, they provide enhanced robustness because the particles can represent multiple position hypotheses. This helps to avoid cases where Kalman filter-based schemes diverge.

B. Simultaneous Localization and Mapping using Multipath Channel Information

How the environment model information can be obtained in practice, remains as a problem. In particular in assisted living scenarios, "plug-and-play" installation is of prime importance. That is, ideally, the environment model has to be acquired "online" while the system is in operation. Simultaneous localization and mapping (SLAM) is a well-known approach to learn a map of the environment with a mobile agent and at the same time to localize the agent within this map [38]. Its application to multipath-assisted indoor localization has been discussed in [34]. In this case, the learned map contains the data of the environment model, the VA positions and the SINR values; i.e. the requirement of plug-and-play installation is fulfilled. In [39], a structure-from-motion approach has been proposed to also estimate the agent and (virtual) anchor locations simultaneously from a set of UWB measurements.

The SLAM algorithm presented in [34] includes map features (the VA positions) within a joint state-space of a tracking filter with the agent and thus updates the VAs whenever new data are available. Again a data association is needed for this purpose, which has been accomplished by a similar subpattern assignment approach as discussed before. Sets of associated past measurements are then used to estimate the current SINR values. Non-associated measurements $\mathcal{Z}_{n,\overline{\text{ass}}}$, on the other hand, are grouped by their delays and used to compute "candidate" VAs that will be included in the environment model, if observed for a sufficiently long time. These new VAs are described by the set $\mathcal{A}_n^{\text{new}}$ shown in Fig 3.

It has been demonstrated in [34] that a 2D-map can be constructed with no prior information about the scenario other than the absolute positions of two fixed anchors. Fig. 5 shows an illustrative example of this SLAM approach, which has been obtained from the same measurement data as the CDFs in Fig. 4. Grey squares indicate the positions of some "expected" VAs computed from the floor plan. Discovered VAs are shown by red (Anchor 1) and blue (Anchor 2) square-cross markers; their marginal position covariance matrices are indicated by standard deviation ellipses, enlarged by a factor of 30 for better visibility. The corresponding true agent trajectory is indicated in grey. The current estimated agent position is shown by the red dot; its standard deviation ellipse is in black (enlarged by a factor of 100).

As shown in the figure—after 68 time steps—a number of relevant VAs have been identified that match very well with the geometrically computed VAs. Some of these VAs have only been associated for a few time steps, corresponding to rather large variances due to large geometric dilution of precision and/or low SINR values (e.g. MPC "A1 door and left window"). On the other hand, some VAs already have converged accurately to their true location (e.g. MPC "A1 blackboard"). Falsely discovered VAs often show a very large variance of their associated amplitudes, corresponding to a low SINR. Thus, their influence on the tracking process remains limited. The overall tracking performance almost matches up the performance of the approach discussed in Fig. 4. 90 % of the errors are within 4.4 cm. Assuming the availability of side information, e.g. from an inertial measurement unit (IMU), we expect that the robustness of this SLAM algorithm against divergence gets even higher.

C. Passive Localization exploiting Multipath

As mentioned above, passive localization has the great advantage that no specific user compliance is necessary—in other words, the person to be helped does not need to remember to carry a specific device. At the same time, the passive principle makes it more challenging to handle multipath. While in an active system, localization can be achieved based on the triangulation with line-of-sight paths, in passive localization we have to base it on "direct paths" that go from the transmitter, via reflection at the target, to the receiver. Furthermore, these "direct paths" are embedded in background paths (paths that propagate from transmitter to receiver without participation of the target—and the delay of the background paths can be larger *or* smaller than those of the direct path. Secondly, there are also indirect paths, which involve reflection at both target and additional objects.

And (analogously to active localization, where the LOS path might be shadowed off), the direct path might be blocked. This overall makes target localization much more difficult.

Despite these difficulties, passive vital sign monitoring has a long history (the main motivation used to be in a military/surveillance context, but the principles can be applied to AL as well). Narrowband Doppler radar was used to detect the presence of breathing already in the 1970s. However, this does not allow to *localize* the breathing person, and is thus of somewhat limited utility for AL applications. A more promising approach seems to be the use of wideband MIMO radar. Ref. [40] demonstrated a prototype that could precisely localize a person and track the small-scale movement of the chest that occurs during breathing from a distance of several meters away. This was enabled with a sounding waveform extending over 7 GHz bandwidth (within the UWB band from 3 to 10 GHz), combined with an 8-element transmit array, and high-resolution (iterative maximum-likelihood estimation) evaluation. Most noteworthy, the localization can be achieved *without* a direct path, as long as the environment (location of walls), etc., is known. The figures in [40] demonstrate the relative location of the echo reflected from head and chest when the target is breathing in or breathing out.

The situation is more difficult when more than one possible target is present. In contrast to active devices that send out unique signatures and thus allow identification of all associated signals, it is difficult (and often impossible) to distinguish between the multipath components belonging to different targets. Such multi-target localization is another difficult but important problem—obviously, in many AL situations (e.g., elder care homes), multiple targets might be present simultaneously, and if they are moving, their trajectories might intersect. From an algorithmic point of view, we have to distinguish the cases where transmitter and receiver have multiple antenna elements (and thus can resolve directions of the echoes), versus the (much more difficult) case of distributed single-antenna transceivers (e.g., [41]).

In addition to localization and tracking, radio signals may be used for the reconstruction of a 3D map of the surrounding environment, e.g. to assist people with impaired vision capabilities. This is of course strongly related to the mapping task of the SLAM approach. The "passive" reflections of the radio waves from the environment are exploited together with additional reflections from targets and walls. A single sensor through-the-wall radar with data association is discussed in [25], multipath-assisted through-the-wall imaging in [26]. The suitability of UWB radars for mapping, imaging, and also breathing detection was shown in [42]. Recently, the concept of the *personal radar* has been proposed as a smartphone-centric low cost solution for the navigation and mapping problem [43]. A personal radar could be an additional feature offered by 5G smartphones, exploiting mm-wave massive antenna arrays with electronic pencil-beam steering capability and high ranging accuracy. The small wavelength of mm-wave technology permits to pack a massive antenna array in pocket-size space [44]. In fact, mm-wave technologies could provide a most suitable platform for the purpose of high-accuracy localization for AL, as discussed next.

IV. MM-WAVE LOCALIZATION SYSTEMS FOR ASSISTED LIVING

Insights gained so far show the promising features of a multipath-assisted indoor localization system. However, the price to pay is a very large signal bandwidth, to enable the separation of MPCs at sufficiently high SINRs. Microwave-band UWB systems can fulfill this promise, but their mass-market adoption seems unlikely, given the recent developments of indoor wireless systems [9]. For conventional wireless systems it would also be possible to utilize the phase evolution of the MPCs for precise localization and tracking [45]. This technique, however, requires large arrays for separating the MPCs at moderate bandwidths and hence might not be relevant in an AL context. 5G wireless systems—on the other hand—will include ultra-wideband radios in the mm-wave frequency band. The IEEE 802.11ad standard [22], for example, already defines an air-interface for a 2 GHz bandwidth system in the 60 GHz frequency band. Beamforming and tracking of MPCs are key elements of such systems. Despite the promising features of mm-wave systems for localization, only few papers address this aspect so far, and even less discuss measurement data and realistic channel models [46], [47].

This section highlights the great potential of mm-wave technologies for realizing multipath-assisted indoor localization. We analyze, for this purpose, exemplary measurement data discussed in [19], [20] that mimic the intended AL application scenario. It is shown that a single access point provides enough position-related information to enable high accuracy localization. A properly parameterized environment model is a key ingredient to achieve this.

A. Measurement Scenario and Setup

The mm-wave channel measurements of [19], [20] are MIMO measurements with 7x7 locations on both TX and RX sides obtained by a vector network analyzer. In the intended application, one array assumes the role of the agent to be localized, while the other corresponds to the anchor, i.e. the fixed infrastructure. (The floorplan is shown in Fig. 7a.) The measurement grid on the agent side was moved to 22 different locations in the room. Both LOS and obstructed LOS (OLOS) situations have been measured; the latter were obtained using a laptop screen to shadow the direct link to the anchor. These measurements have been conducted at a center frequency of 63 GHz. To mimic the IEEE 802.11ad standard [22], we selected a subband of 2 GHz from the total measured bandwidth of 4 GHz, using a raised cosine filter (cf. [33]).

B. Measurement Results

We first analyze the SINRs of the MPCs as defined in (2), i.e. the ratio of the useful energies of the deterministic MPCs to the interference by DM and AWGN. The SINRs are estimated using the technique of [18], [33], a method-of-moments estimator operating directly on the MPC amplitudes. In this way, the PDP $S_\nu(\tau)$ does not explicitly have to be estimated. We use the array positions on the anchor-side to provide the required signal ensemble. The array at the agent-side is used to show the potential of beamforming. In a

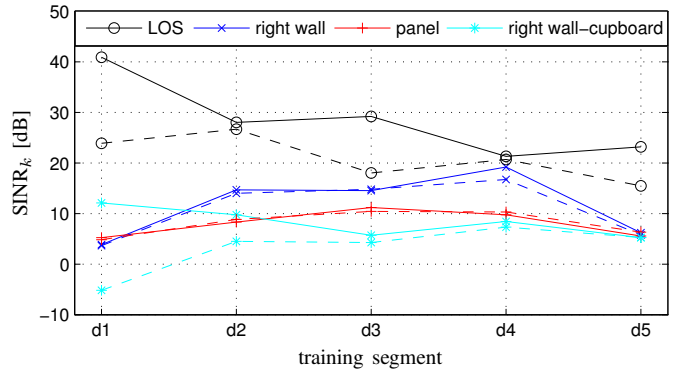

(a) SINR of MPCs

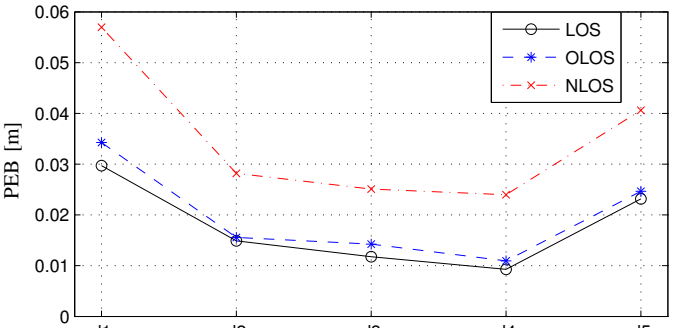

(b) PEB for LOS/OLOS/NLOS

Fig. 6. (a) Estimated SINRs of selected reflections using $T_\mathrm{p} = 0.5\,\mathrm{ns}$ and $f_\mathrm{c} = 63\,\mathrm{GHz}$ and (b) PEB for LOS, OLOS, and NLOS (complete lack of the LOS component) scenarios. Solid lines indicate LOS measurements; while dashed and dash-dotted lines correspond to OLOS and NLOS measurements, respectively. The x-axis labeling refers to the measurement sets acquired at different positions $d_1, \ldots, d_5$ as reported in [19], [20].

practical setup, it may be advantageous to implement the beamforming at the anchor side, i.e. at the infrastructure, where the array has a known orientation, while at the agent side, low-complexity terminals may be used that have only one or a few fixed antennas. We reverse these roles here, since the horizontal array geometry at the agent-side was better suited for a proof-of-principle.

The *estimated SINRs* in Fig. 6a show the relevance of selected MPCs in this environment for several agent positions. The LOS is the MPC providing most position-related information. Besides the fact that it is usually the strongest component of a radio channel, this significance is due to the relatively low impact of DM on the LOS component at a bandwidth of 2 GHz [33]. Interestingly, in some cases, the SINR of the LOS component drops only slightly in the OLOS situation, although its energy drops significantly (the average LOS K-factor over the estimation positions decreases from $8.9\,\mathrm{dB}$ to $-7.4\,\mathrm{dB}$). This implies that the component is still exploitable for localization. The reflected components also show significant SINRs over the estimation points but there is quite some location-dependence of the SINRs. It is more pronounced than for microwave band UWB measurements [33], highlighting the need for online estimation (tracking) of the environment model, as explained in Section III-B and [34].

Fig. 6b shows the PEB (the square root of the trace of the inverse of the EFIM (3)) corresponding to the estimated SINRs of Fig. 6a. The PEB is a measure of the potentially achievable localization accuracy, hence highly-accurate single-anchor localization is possible in this scenario. The PEB increases only slightly in the OLOS situations, due to the still significant SINR of the LOS component. Even if the LOS component is not taken into account at all, (NLOS; the red dash-dotted line), the agent is still localizable at centimeter level, easily satisfying requirements of most AL applications. A proper operation in total absence of an LOS indicates the "good" robustness of the discussed techniques.

Fig. 7 shows the likelihood (4) for a sampled received signal $r(t)$ as a function of position $\mathbf{p}$, evaluated over the floorplan. It compares (a) LOS and (b) OLOS conditions with (c) OLOS with the use of beamforming. The bold black lines indicate the directions to the anchor, thin black lines the directions to first-order VAs, and black dashed lines the directions to second-order VAs. The black diamonds mark the estimated positions of the agent. Using a maximum likelihood positioning algorithm as in [24], an error in the centimeter level is achieved ($2\,\mathrm{cm}$ for the LOS and $3\,\mathrm{cm}$ for the OLOS situations). Only a small degradation results in the OLOS case, as anticipated from the analysis of the SINR values.

The potential use of beamforming shows a different great advantage: the multimodality of the likelihood function is reduced, which reduces the risk of converging to a wrong local maximum. Large modes at locations farther away from the true agent position are suppressed due to the angular resolution of the array antenna. Note, however, that MPC delays are still responsible for providing a high accuracy in a direction orthogonal to the LOS path. Without the processing of multipath, we would see a smooth maximum (along the circle) in stead of a sharp peak. The likelihood function in Fig. 7c has been computed by using a phased-array beamformer for each exploited MPC. This is achieved by coherently adding the signals at the agent-side array positions, taking into account the relative phase shifts that correspond to the known arrival angles of the MPCs. The figure exemplary shows that such a processing, envisioned for 5G mm-wave communication systems, can greatly improve the robustness of the localization, since many local maxima can be ruled out.

V. Discussion and Conclusion

This paper envisions accurate and robust indoor localization as a key sensing modality of an AL systems. It has been shown that awareness to the signal propagation conditions enables the robustness and allows to reduce the needed infrastructure. Experimental, measurement-based results support the discussion of theoretical findings.

A geometry-based stochastic model of the received signal allows the derivation of theoretical position error bounds and thus provides the theoretical background for a number of multipath-assisted localization and tracking algorithms. More specifically, an environment model, consisting of a geometrical model (based on VA positions) and a measurement uncertainty model (based on the SINR of MPCs), yields insight in the potential location information that can be acquired at a

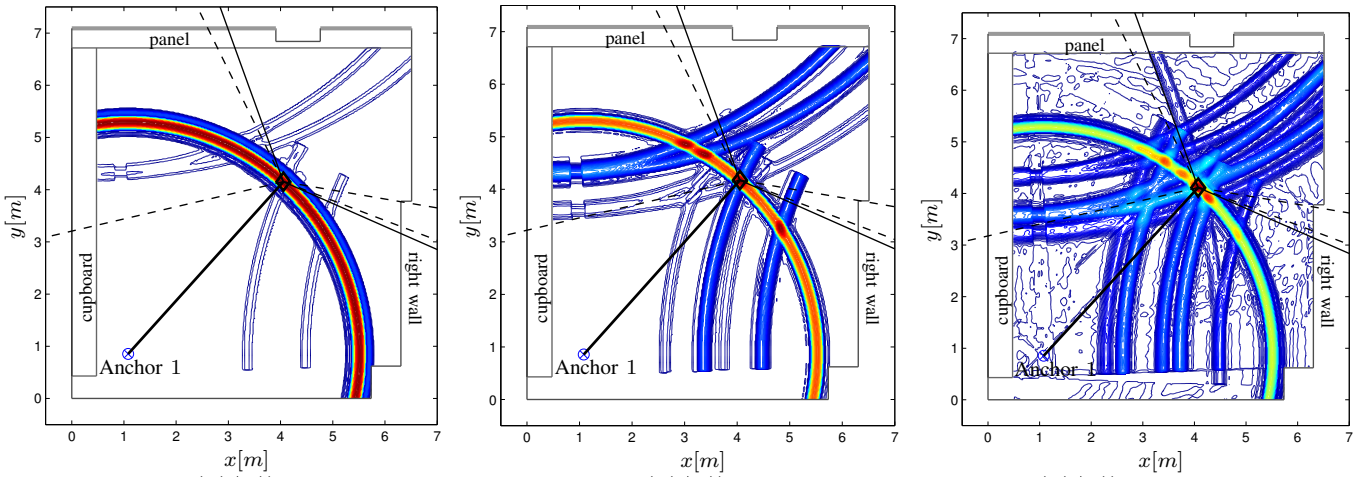

(a) $\log(p(\mathbf{r}|\boldsymbol{\psi}))$ LOS (b) $\log(p(\mathbf{r}|\boldsymbol{\psi}))$ OLOS (c) $\log(p(\mathbf{r}|\boldsymbol{\psi}))$ OLOS, beamforming

Fig. 7. Likelihood function over the floor plan for (a) LOS, (b) OLOS situation, and (c) OLOS situation with phased-array beamforming. The position error of the MLE is 2 cm and 3 cm for LOS and OLOS situations, respectively. Bold black lines show the directions to the anchors, thin black line the directions to first-order VAs, and black dashed lines the directions to second-order VAs. The black diamonds mark the estimated positions of the agent.

certain position, in a certain environment. Several algorithms have been discussed that exploit such information: Maximum likelihood localization, tracking filters with data association, and algorithms for passive localization. The benefit of using this environmental information has been shown.

Future 5G mm-wave communication systems could be an ideal platform for achieving high-accuracy indoor localization with this concept. In addition to a large signal bandwidth, beamforming capabilities are envisioned for such systems, which can be exploited to make the localization and tracking more robust and efficient. It becomes feasible to obtain accurate and robust indoor localization with only a single anchor node in a room, with a system that also serves as a standard-compliant access point for 5G communications.

Note that vice-versa the environment model can be exploited by the communications system. "Location awareness" is created by providing a site-specific propagation model that can be used to improve the robustness of the radio air-interface. For example the arrival and departure angles of the most significant radio paths are encoded in the environment model, which will be useful for efficient beamsteering algorithms for communications in highly dynamic environments, extending the scope of the proposed concepts well beyond AL scenarios.

Proposed Call-outs

- A cm-accuracy indoor positioning system *alone* enables a wide range of AL applications.
- Radio technology is promising for positioning as low-power transceivers can be built at small size.
- Awareness to the signal propagation conditions enables robustness and reduces the requirements on the infrastructure.
- Multipath-assisted methods enable high-accuracy indoor localization with only a single 5G access point in a room.

Appendix

Boxed block: Derivation of the PEB

This appendix is a placeholder for a text box on statistical signal modeling and CRLB derivation that can be separated from the main text.

The Cramér-Rao bound is a lower bound on the error variance of a parameter estimator. It is obtained from the second derivative of the log of the measurement likelihood function w.r.t. the estimation parameters, quantifying the curvature of this likelihood function. For an unbiased estimator, this curvature relates to the potential measurement precision [48]. Assuming zero-mean complex Gaussian noise processes, a likelihood function derived from a discrete-time version of the signal model (1) can be written as

$$f(\mathbf{r}|\boldsymbol{\psi}) \propto \exp\left\{-(\mathbf{r}-\mathbf{S}\boldsymbol{\alpha})^{\mathrm{H}}{\mathbf{C_n}}^{-1}(\mathbf{r}-\mathbf{S}\boldsymbol{\alpha})\right\} \qquad (4)$$

where $\mathbf{r}$ is the received signal sampled at rate $1/T_\mathrm{s}$, the parameter vector $\boldsymbol{\psi} = [\boldsymbol{\alpha}^T,\ \boldsymbol{\tau}^T]^T$ stacks the complex amplitudes $\{\alpha_k\}$ and delays $\{\tau_k\}$, $\mathbf{S} = [\mathbf{s}_{\tau_1}, \ldots, \mathbf{s}_{\tau_K}] \in \mathbb{R}^{N\times K}$ is the signal matrix containing delayed versions $\mathbf{s}_{\tau_k} = [s(-\tau_k), s(T_\mathrm{s}-\tau_k), \ldots, s((N-1)T_\mathrm{s}-\tau_k)]^\mathrm{T}$ of the sampled transmit pulse, and the matrix $\mathbf{C_n} = {\sigma_\mathrm{n}}^2\mathbf{I}_N + \mathbf{C_c} \in \mathbb{R}^{N\times N}$ denotes the co-variance matrix of the noise processes. The elements of the DM co-variance matrix are given by $[\mathbf{C_c}]_{n,m} = T_\mathrm{s}\sum_{i=0}^{N-1} S_\nu(iT_\mathrm{s})s(nT_\mathrm{s}-iT_\mathrm{s})s(mT_\mathrm{s}-iT_\mathrm{s})$; the AWGN samples have variance ${\sigma_\mathrm{n}}^2 = N_0/T_\mathrm{s}$.

A number of analytical manipulations are needed to obtain the insightful expressions (2) and (3) for the CRLB[4]. The difficulty lies in finding the inverse of the covariance matrix $\mathbf{C_n}$. Under the assumption that the useful components in (1) are non-overlapping, it is fair to assume that each of these

[4]It can be intuitively argued that (4) satisfies the regularity condition required for the CRLB derivation [48] for all points within the room: Considering a correct geometry and a sufficiently large signal bandwidth, the likelihood has a maximum at the true position whose spatial extent is small w.r.t. the room dimensions. It can be shown that the regularity condition is satisfied even without these assumptions, but this is out of scope here.

components can be observed independently. The DM process is then treated as stationary for each MPC at a variance defined by the PDP at the MPC's corresponding excess delay, $S_\nu(\tau_k)$. We can then use the Fourier transform to compute the inverse and obtain for the Fisher information of the k-th delay estimate the expression [27]

$$\begin{aligned}\mathbb{E}_{\mathbf{r}|\boldsymbol{\psi}}\left\{-\frac{\partial^2 \ln f(\mathbf{r}|\boldsymbol{\psi})}{\partial\tau_k\partial\tau_k}\right\} &\approx 8\pi^2|\alpha_k|^2 \\ &\int_f f^2 \frac{|\mathrm{S}(f)|^2}{N_0 + S_\nu(\tau_k)|\mathrm{S}(f)|^2}\mathrm{d}f \\ &\overset{(\mathrm{BS})}{=} 8\pi^2 \mathrm{SINR}_k \int_f f^2 |\mathrm{S}(f)|^2 \mathrm{d}f \\ &= 8\pi^2\beta^2\mathrm{SINR}_k\end{aligned} \tag{5}$$

where $\beta^2 = \int_f f^2|S(f)|^2\mathrm{d}f$ is the mean square bandwidth of (the Fourier transform $S(f)$ of) pulse $s(t)$, $\mathrm{SINR}_k = |\alpha_k|^2/(N_0 + T_\mathrm{p}S_\nu(\tau_k))$ is the signal-to-interference-plus-noise ratio (SINR) of the k-th MPC. The second line only holds for a block spectrum (BS) $|S(f)|^2 = T_\mathrm{p}$ for $|f| \leq 1/(2T_\mathrm{p})$; a generalized version of this equation has been derived in [27].

To compute the *equivalent* Fisher information matrix (EFIM) *for the position vector* from the Fisher information matrix of the parameter vector $\boldsymbol{\psi}$, we evoke the matrix inversion lemma to account for the nuisance parameters $\{\alpha_k\}$ and a parameter transformation to convert the delays $\{\tau_k\}$ to the position vector $\mathbf{p}$ [30]. The latter requires the computation of the Jacobian $\mathbf{H} = \partial\boldsymbol{\tau}/\partial\mathbf{p}$, the derivative of the delays $\{\tau_k\}$ w.r.t. position $\mathbf{p}$. It describes the variation of the delays w.r.t. the position and can assume different, scenario-dependent forms, depending on the roles of anchors and agents. General expressions for these *spatial delay gradients* have been derived in [27]. For an MPC arriving from direction ϕ_k we get $\partial\tau_k/\partial\mathbf{p} = \mathbf{e}(\phi_k)$ with unit-norm vector $\mathbf{e}(\phi_k)$ pointing in direction ϕ_k, which leads to the matrices $\mathbf{J}_r(\phi_k) = \mathbf{e}(\phi_k)\mathbf{e}^\mathrm{T}(\phi_k)$ in (3).

REFERENCES

[1] G. Acampora, D. Cook, P. Rashidi, and A. Vasilakos, "A survey on ambient intelligence in healthcare," *Proceedings of the IEEE*, vol. 101, no. 12, pp. 2470–2494, Dec 2013.

[2] P. Barsocchi, S. Chessa, F. Furfari, and F. Potorti, "Evaluating Ambient Assisted Living Solutions: The Localization Competition," *IEEE Pervasive Computing*, vol. 12, no. 4, pp. 72–79, Oct 2013.

[3] P. Rashidi and A. Mihailidis, "A Survey on Ambient-Assisted Living Tools for Older Adults," *IEEE Journal of Biomedical and Health Informatics*, vol. 17, no. 3, pp. 579–590, May 2013.

[4] M. Z. Win, A. Conti, S. Mazuelas, Y. Shen, W. M. Gifford, D. Dardari, and M. Chiani, "Network Localization and Navigation via Cooperation," *IEEE Commun. Mag.*, vol. 49, no. 5, pp. 56–62, May 2011.

[5] S. Gezici, Z. Tian, G. B. Giannakis, H. Kobayashi, A. F. Molisch, H. V. Poor, and Z. Sahinoglu, "Localization via Ultra-wideband Radios: A Look at Positioning Aspects for Future Sensor Networks," *IEEE Signal Process. Mag.*, vol. 22, no. 4, pp. 70–84, Jul. 2005.

[6] S. Bartoletti, W. Dai, A. Conti, and M. Z. Win, "A Mathematical Model for Wideband Ranging," *IEEE J. Sel. Topics Signal Process.*, vol. 9, no. 2, pp. 216–228, Mar. 2015.

[7] D. Dardari, A. Conti, U. J. Ferner, A. Giorgetti, and M. Z. Win, "Ranging with Ultrawide Bandwidth Signals in Multipath Environments," *Proc. IEEE*, vol. 97, no. 2, pp. 404–426, Feb. 2009.

[8] H. Wymeersch, J. Lien, and M. Z. Win, "Cooperative Localization in Wireless Networks," *Proceedings of the IEEE*, vol. 97, no. 2, pp. 427–450, 2009.

[9] A. Conti, M. Guerra, D. Dardari, N. Decarli, and M. Win, "Network experimentation for cooperative localization," *IEEE Journal on Selected Areas in Communications*, vol. 30, no. 2, pp. 467–475, 2012.

[10] S. Bartoletti, A. Giorgetti, M. Z. Win, and A. Conti, "Blind Selection of Representative Observations for Sensor Radar Networks," *IEEE Trans. Veh. Technol.*, vol. 64, no. 4, pp. 1388–1400, Apr. 2015.

[11] B. U. Töreyin, Y. Dedeoğlu, and A. Çetin, "HMM based falling person detection using both audio and video," in *Computer Vision in Human-Computer Interaction*, ser. Lecture Notes in Computer Science, N. Sebe, M. Lew, and T. Huang, Eds. Springer Berlin Heidelberg, 2005, vol. 3766, pp. 211–220.

[12] D. Weinland, R. Ronfard, and E. Boyer, "A survey of vision-based methods for action representation, segmentation and recognition," *Computer Vision and Image Understanding*, vol. 115, no. 2, pp. 224 – 241, 2011. [Online]. Available: http://www.sciencedirect.com/science/article/pii/S1077314210002171

[13] Y. Li, K. Ho, and M. Popescu, "A microphone array system for automatic fall detection," *Biomedical Engineering, IEEE Transactions on*, vol. 59, no. 5, pp. 1291–1301, May 2012.

[14] M. Z. Win and R. A. Scholtz, "Impulse radio: How it works," *IEEE Commun. Lett.*, vol. 2, no. 2, pp. 36–38, Feb. 1998.

[15] ——, "Ultra-Wide Bandwidth Time-Hopping Spread-Spectrum Impulse Radio for Wireless Multiple-Access Communications," *IEEE Trans. Commun.*, vol. 48, no. 4, pp. 679–691, Apr. 2000.

[16] ——, "Characterization of Ultra-Wide Bandwidth Wireless Indoor Communications Channel: A Communication-Theoretic View," *IEEE J. Sel. Areas Commun.*, vol. 20, no. 9, pp. 1613–1627, Dec. 2002.

[17] A. F. Molisch, D. Cassioli, C.-C. Chong, S. Emami, A. Fort, B. Kannan, J. Karedal, J. Kunisch, H. Schantz, K. Siwiak, and M. Z. Win, "A Comprehensive Standardized Model for Ultrawideband Propagation Channels," *IEEE Trans. Antennas Propag.*, vol. 54, no. 11, pp. 3151–3166, Nov. 2006.

[18] P. Meissner, E. Leitinger, and K. Witrisal, "UWB for Robust Indoor Tracking: Weighting of Multipath Components for Efficient Estimation," *IEEE Wireless Communications Letters*, vol. 3, no. 5, pp. 501–504, Oct. 2014.

[19] S. Wyne, K. Haneda, S. Ranvier, F. Tufvesson, and A. Molisch, "Beamforming Effects on Measured mm-Wave Channel Characteristics," *IEEE Transactions on Wireless Communications*, vol. 10, no. 11, pp. 3553–3559, November 2011.

[20] C. Gustafson, K. Haneda, S. Wyne, and F. Tufvesson, "On mm-Wave Multipath Clustering and Channel Modeling," *IEEE Transactions on Antennas and Propagation*, vol. 62, no. 3, pp. 1445–1455, March 2014.

[21] A. Molisch and F. Tufvesson, "Propagation channel models for next-generation wireless communications systems," *IEICE Transactions on Communications*, vol. E97B, no. 10, pp. 2022–2034, 2014.

[22] *ISO/IEC/IEEE International Standard for Information technology–Telecommunications and information exchange between systems–Local and metropolitan area networks–Specific requirements-Part 11: Wireless LAN Medium Access Control (MAC) and Physical Layer (PHY) Specifications Amendment 3: Enhancements for Very High Throughput in the 60 GHz Band (adoption of IEEE Std 802.11ad-2012)*, IEEE Std., 2014.

[23] R. Di Taranto, S. Muppirisetty, R. Raulefs, D. Slock, T. Svensson, and H. Wymeersch, "Location-Aware Communications for 5G Networks: How location information can improve scalability, latency, and robustness of 5G," *IEEE Signal Processing Magazine*, vol. 31, no. 6, pp. 102–112, Nov 2014.

[24] E. Leitinger, M. Froehle, P. Meissner, and K. Witrisal, "Multipath-Assisted Maximum-Likelihood Indoor Positioning using UWB Signals," in *IEEE ICC Workshop on Advances in Network Localization and Navigation (ANLN)*, 2014, pp. 170–175.

[25] P. Setlur, G. Smith, F. Ahmad, and M. Amin, "Target Localization with a Single Sensor via Multipath Exploitation," *IEEE Transactions on Aerospace and Electronic Systems*, vol. 48, no. 3, pp. 1996–2014, July 2012.

[26] M. Leigsnering, M. Amin, F. Ahmad, and A. Zoubir, "Multipath Exploitation and Suppression for SAR Imaging of Building Interiors: An overview of recent advances," *IEEE Signal Processing Magazine*, vol. 31, no. 4, pp. 110–119, 2014.

[27] E. Leitinger, P. Meissner, C. Ruedisser, G. Dumphart, and K. Witrisal, "Evaluation of position-related information in multipath components for indoor positioning," *IEEE Journal on Selected Areas in Communications*, vol. 33, no. 11, pp. 2313–2328, Nov 2015.

[28] Y. Shen and M. Win, "On the Use of Multipath Geometry for Wideband Cooperative Localization," in *IEEE Global Telecommunications Conference (GLOBECOM)*, 2009, pp. 1–6.

[29] D. B. Jourdan, D. Dardari, and M. Z. Win, "Position Error Bound for UWB Localization in Dense Cluttered Environments," *IEEE Trans. Aerosp. Electron. Syst.*, vol. 44, no. 2, pp. 613–628, Apr. 2008.

[30] Y. Shen and M. Win, "Fundamental Limits of Wideband Localization; Part I: A General Framework," *IEEE Transactions on Information Theory*, vol. 56, no. 10, pp. 4956–4980, 2010.

[31] Y. Shen, H. Wymeersch, and M. Win, "Fundamental Limits of Wideband Localization - Part II: Cooperative Networks," *IEEE Transactions on Information Theory*, vol. 56, no. 10, pp. 4981–5000, 2010.

[32] Y. Qi, H. Kobayashi, and H. Suda, "Analysis of wireless geolocation in a non-line-of-sight environment," *IEEE Transactions on Wireless Communications*, vol. 5, no. 3, pp. 672–681, 2006.

[33] P. Meissner, "Multipath-Assisted Indoor Positioning," Ph.D. dissertation, Graz University of Technology, 2014.

[34] E. Leitinger, P. Meissner, M. Lafer, and K. Witrisal, "Simultaneous Localization and Mapping using Multipath Channel Information," in *IEEE ICC Workshop on Advances in Network Localization and Navigation (ANLN)*, June 2015, pp. 754–760.

[35] D. Schuhmacher, B.-T. Vo, and B.-N. Vo, "A Consistent Metric for Performance Evaluation of Multi-Object Filters," *IEEE Transactions on Signal Processing*, vol. 56, no. 8, pp. 3447–3457, 2008.

[36] S. Haykin, "Cognitive radar: a way of the future," *IEEE Signal Process. Mag.*, vol. 23, pp. 30–40, Jan. 2006.

[37] K.Witrisal, E. Leitinger, P. Meissner, and D. Arnitz, "Cognitive radar for the localization of RFID transponders in dense multipath environments," in *IEEE Radar Conference*, Ottawa, Canada, Apr. 2013.

[38] H. Durrant-Whyte and T. Bailey, "Simultaneous localization and mapping: part I," *Robotics & Automation Magazine, IEEE*, vol. 13, no. 2, pp. 99–110, June 2006.

[39] Y. Kuang, K. Astrom, and F. Tufvesson, "Single antenna anchor-free UWB positioning based on multipath propagation," in *IEEE International Conference on Communications (ICC)*, June 2013, pp. 5814–5818.

[40] J. Salmi and A. F. Molisch, "Propagation Parameter Estimation, Modeling and Measurements for Ultrawideband MIMO Radar," *IEEE Transactions on Antennas and Propagation*, vol. 59, no. 11, pp. 4257–4267, 2011.

[41] J. Shen and A. Molisch, "Estimating multiple target locations in multipath environments," *IEEE Transactions on Wireless Communications*, vol. 13, no. 8, pp. 4547–4559, 2014.

[42] R. Zetik, J. Sachs, and R. Thoma, "UWB short-range radar sensing - The architecture of a baseband, pseudo-noise UWB radar sensor," *IEEE Instrumentation Measurement Magazine*, vol. 10, no. 2, pp. 39–45, April 2007.

[43] F. Guidi, A. Guerra, and D. Dardari, "Personal Mobile Radars with Millimeter-Wave Massive Arrays for Indoor Mapping," *IEEE Transactions on Mobile Computing*, vol. PP, no. 99, pp. 1–1, 2015.

[44] W. Hong, K.-H. Baek, Y. Lee, Y. Kim, and S.-T. Ko, "Study and prototyping of practically large-scale mmWave antenna systems for 5G cellular devices," *IEEE Commun. Mag.*, vol. 52, no. 9, pp. 63–69, Sep. 2014.

[45] M. Zhu, J. Vieira, Y. Kuang, K. Astrom, A. F. Molisch, and F. Tufvesson, "Tracking and positioning using phase information from estimated multipath components," in *IEEE ICC Workshop on Advances in Network Localization and Navigation (ANLN)*, London, UK, Jun. 2015, pp. 712–717.

[46] H. El-Sayed, G. Athanasiou, and C. Fischione, "Evaluation of localization methods in millimeter-wave wireless systems," in *IEEE 19th International Workshop on Computer Aided Modeling and Design of Communication Links and Networks (CAMAD)*, Dec 2014, pp. 345–349.

[47] A. Guerra, F. Guidi, and D. Dardari, "Position and orientation error bound for wideband massive antenna arrays," in *IEEE ICC Workshop on Advances in Network Localization and Navigation (ANLN)*, 2015, pp. 853–858.

[48] S. Kay, *Fundamentals of Statistical Signal Processing: Estimation Theory*. Prentice Hall Signal Processing Series, 1993.